Electronic Supplementary Material (ESI) for Materials Advances.

Exploring the Effects of Synthesis Parameters on the Properties and Photoactivity of WO_3-graphene oxide Synthesized via Microwave Route

*Bárbara S. Rodrigues,[a] Markus Niederberger and Juliana S. Souza[a]**

[a]Centro de Ciências Naturais e Humanas, Universidade Federal do ABC, 09210-580, Santo André, SP, Brazil.

[b]Laboratory for Multifunctional Materials, Department of Materials, ETH Zurich, 8093, Zurich,, Switzerland.

Supporting Information

Synthesis of WO_3 modified with various proportions of GO

0.5 mmol of tungsten hexachloride (WCl_6) was diluted in 200 µL of methanol in a borosilicate microwave vial of 10 mL, and the mixture was stirred for 2h. At the same time, 100 mg of graphene oxide was suspended in 20 mL of benzyl alcohol and sonicated for 2h, forming a black suspension.

The GO suspension was added into the microwave vial according to the proportion of GO desired, and the volume of the flask was completed with benzyl alcohol to 4 mL of precursor in each vial. The precursors were inserted in a microwave cavity and irradiated for 1 min at 180°C and for 10 min up to 200 °C, as reported previously in the literature[1,2].

The proportion of graphene oxide added to the reactional media was investigated to optimize one condition. Many authors stated that around 1 - 4% wt. of graphene oxide is ideal for enhancing electron conduction without reducing photoactivity[3,4]. Also, graphene oxide is an opaque black powder that may absorb the most visible light, which would be inconvenient for photocatalytic purposes [5]. Therefore, a rough estimation of the electron percolation threshold of GO was made. This value is related to the volume of filler (in this case, graphene materials: graphene oxide - GO or reduced graphene oxide - rGO) necessary to create an electron pathway increasing the conductivity of a ceramic material. Markandan and collaborators (2017)[6] have shown that for most reported oxides the value is between 3 – 9% v/v. Since the density of GO bought from Sigma Aldrich is 1.8 g cm^{-3}, the density of WO_3 is 7.2 g cm^{-3}, and the mass of WO_3 produced is around 140 mg, it is possible to calculate the volume of filler through Equation S1.

Equation S1

$$\rho = \frac{m}{V}$$

Where ρ is the density, m is related to the mass and v is the calculated volume of graphene oxide. Then, the amount of GO added to the synthesis should be between 0.5 and 3% (wt) of the amount of WO_3 produced. A saturation condition was also created to compare if increasing the amount of graphene up to 10% changes the physical-chemical properties of the materials. Therefore, the samples were named WO_3, $WO_3$0.5%GO, $WO_3$3%GO and $WO_3$10%GO.

Analyzing the XRD (Figure SI-1 a), it is possible to observe that the crystalline phase identified for the pristine sample did not change by adding graphene. In addition, it is not

possible to identify any peak associated with graphene or GO. This feature is expected and often reported in the literature since the reduction of graphene can be microwave-induced [7,8]. It may reduce the crystallinity degree of graphene due to the enhancement of structural defects on the lattice [9,10]. Furthermore, the low GO content also has been reported as a cause for the absence of its characteristic peaks [11].

The region of the main intense peaks of monoclinic WO_3 diffractogram around 24.2° was expanded (Figure SI – 1b). It has shown almost no difference regarding the peak position, intensity and wideness between the peak of pristine WO_3 and $WO_3$0.5%GO. However, adding 3% of GO enhances the intensity and the resolution of the shoulder found at 23.6° (Figure SI - 1b). While overloading the WO_3 with graphene, instead of promoting an even better resolution of this peak, leads to an enlargement of the main peak. This can be associated with the formation of smaller crystallites or an amorphous phase [12].

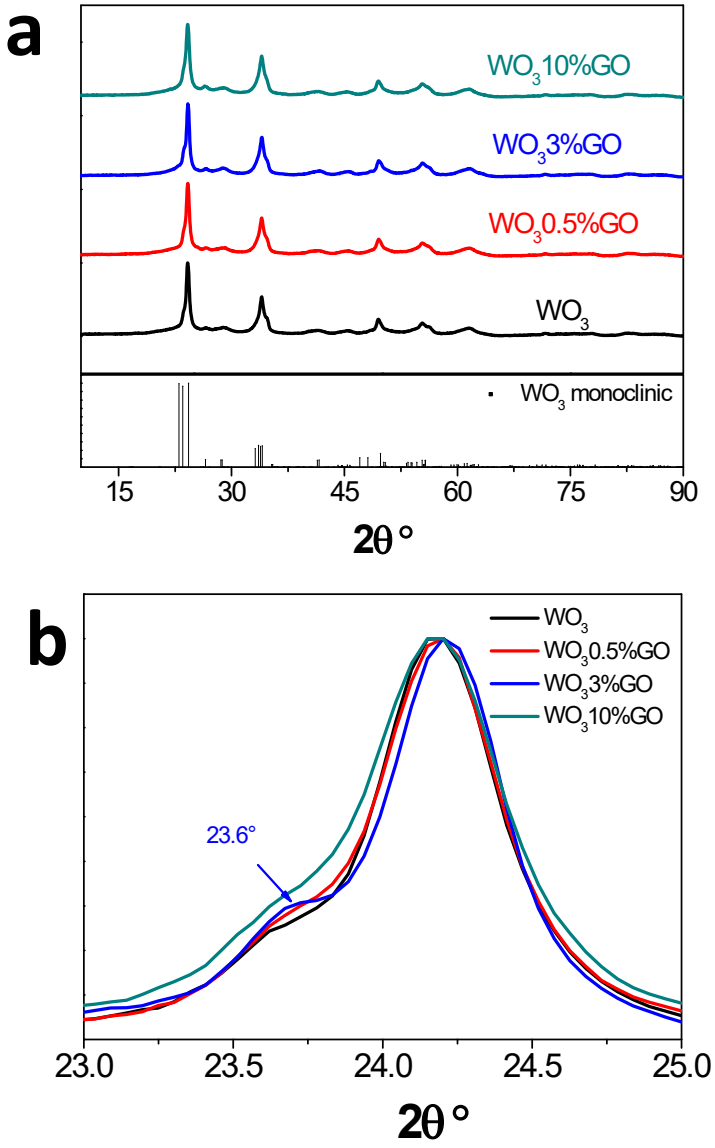

Figure SI - 1. (a) XRD of $WO_3$0.5%GO; $WO_3$3%GO and $WO_3$10%GO, (b) magnified reflection around the main peak at 23.5°.

The morphology observed for tungsten oxide did not change either by loading it with GO), as followed at SI – 2a. WO_3 exhibited a nanoplatelets shape that was also observed in the sample $WO_3$3%GO (Figure SI- 2 b). However, GO can also form small plates. Thus, the structures with irregular edges could also be particles of GO. $WO_3$10%GO has also exhibited the nanoplatelets morphology. In this case, some bigger structures might be associated with GO (Figure SI – 2 c), which coincides with the SEM images of GO (Figure SI- 2 d) that showed plate-like particles non-homogeneous in size.

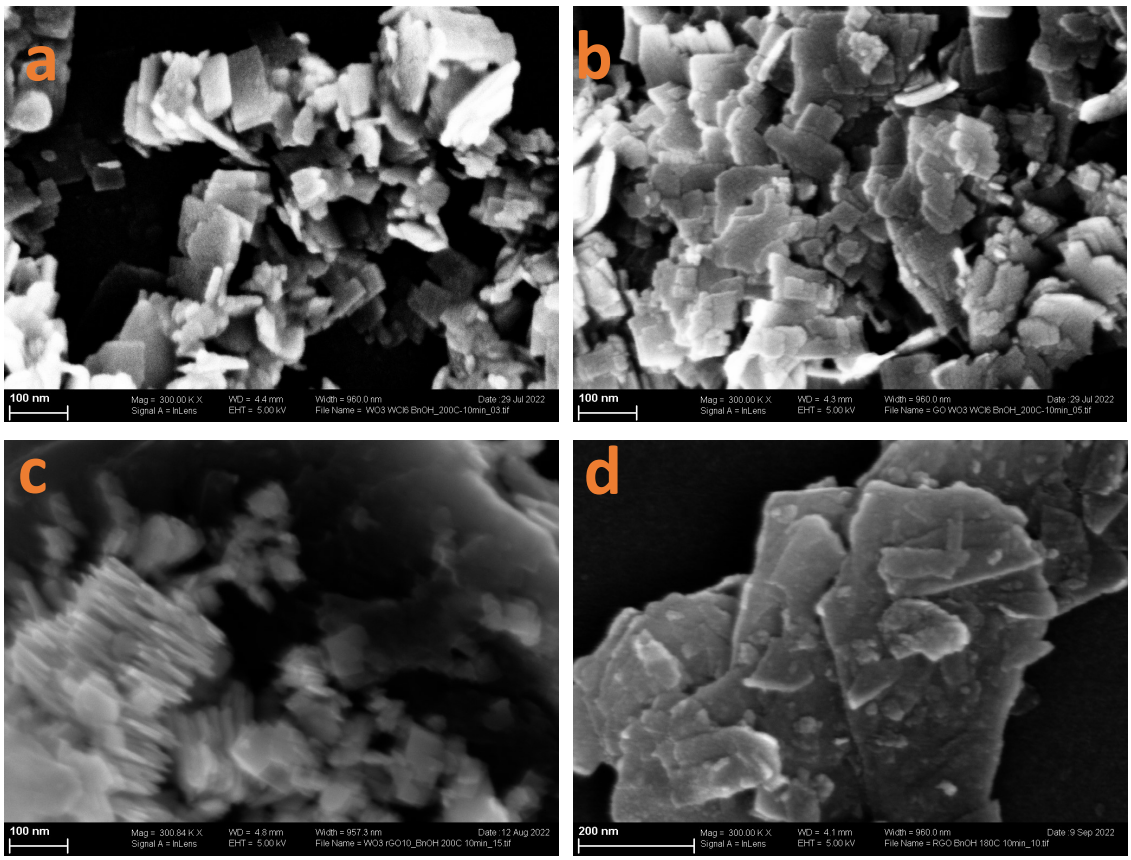

Figure SI - 2. SEM images at high and low magnifications of (a) pristine WO_3, (b) $WO_3$3%GO, (c) $WO_3$10%GO and (d) pristine GO.

N_2 adsorption/desorption isotherm shows evidence of mesoporosity in WO_3 sample (Figure SI – 3 a) that is associated with the type IV isotherm according to IUPAC classification with a characteristic hysteresis loop (type H1) [13]. On the other hand, GO (Figure SI - 3 c) has shown N_2 adsorption/desorption curves that resembles the type II isotherm with the hysteresis of the type H3 that is usually related to slit-shaped pores [13,14]. The same type of hysteresis was observed for $WO_3$3%GO, however with type IV isotherm, which is coincident with pristine WO_3[15].

According to Salama and collaborators (2019)[15], this might be an effect of GO incorporation into WO_3. However, BET (Figures SI 3 b, d and e) has shown that the incorporation of GO did not change the surface area of $WO_3$3%GO, even though the surface area of bare graphene is considerably larger. This leads us to three hypotheses: (i) the proportion of GO added is not enough to increase the surface area overall; (ii) the graphene is homogeneously dispersed between the WO_3 particles, therefore that are no large and isolated graphene particles to promote the increase of surface area; (iii) the microwave synthesis reduces the number of pores of GO.

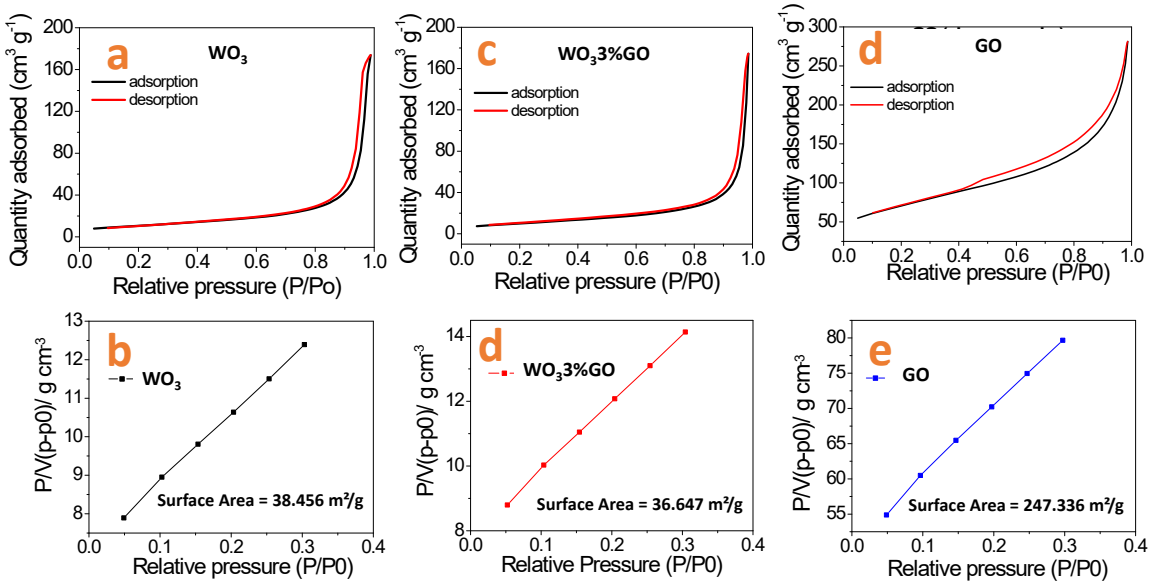

Figure SI - 3. N_2 adsorption and desorption isotherms and BET of WO_3 (a) and (b), $WO_3$3%GO (c) and (d), and GO (e) and (f), respectively.

Since the color of the samples changed from green-yellow to gray due to the presence of graphene oxide, the optical absorption spectra also changed (Figure SI -4). The optical absorption was measured through UV−vis spectroscopy using a JASCO V-770 spectrophotometer with an ILN-725 integrating sphere. In this sense, we observed that the material with 10% graphene oxide exhibits an intense absorption even at higher wavelength values. However, such a trend was not observed for the samples with a lower concentration of graphene oxide, $WO_3$0.5%GO and $WO_3$3%GO. Considering that such an increased absorption of photons non-associated with electron transitions would probably harm the photocatalytic process[5], the selected condition for further investigations was $WO_3$3%GO.

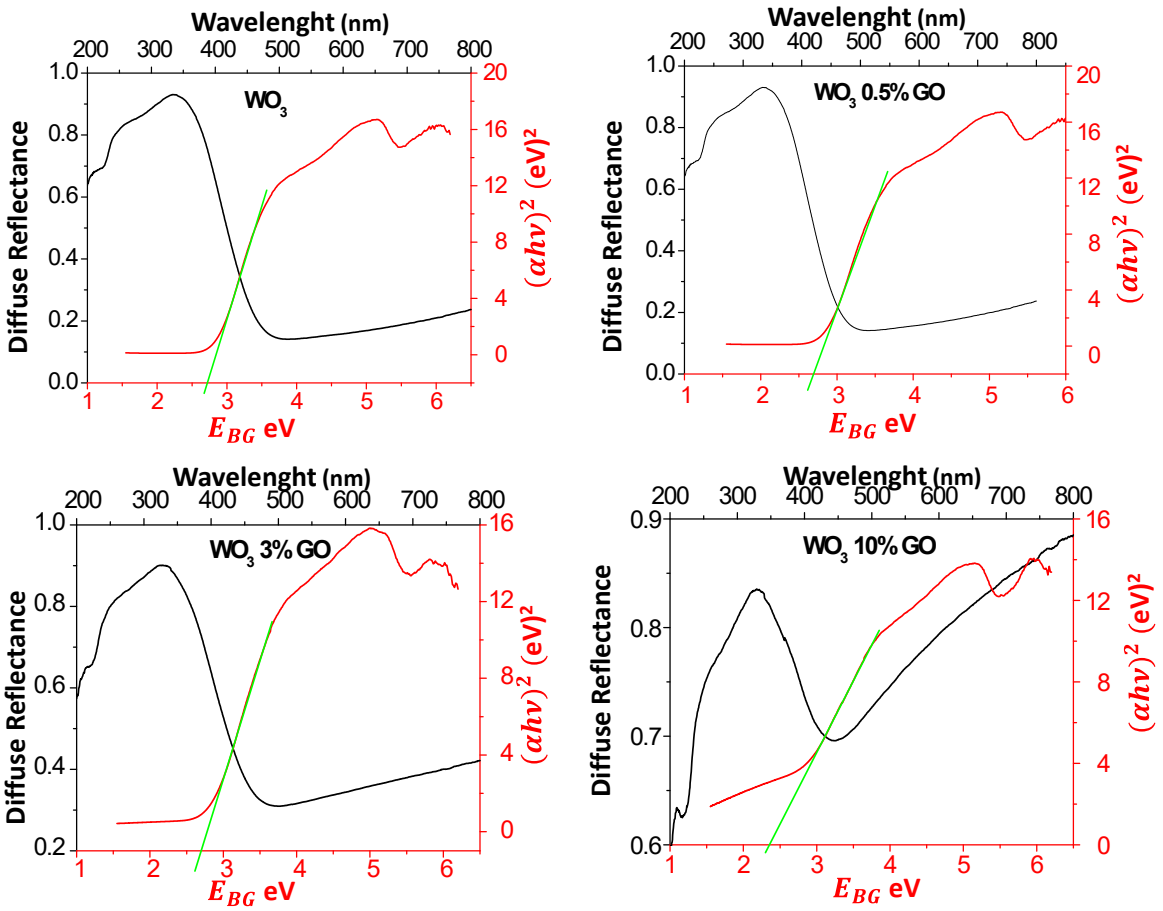

Figure SI - 4. Diffuse reflectance and Tauc Plot of samples WO_3, $WO_3$0.5%GO, $WO_3$3%GO and $WO_3$10%GO.

STEM images

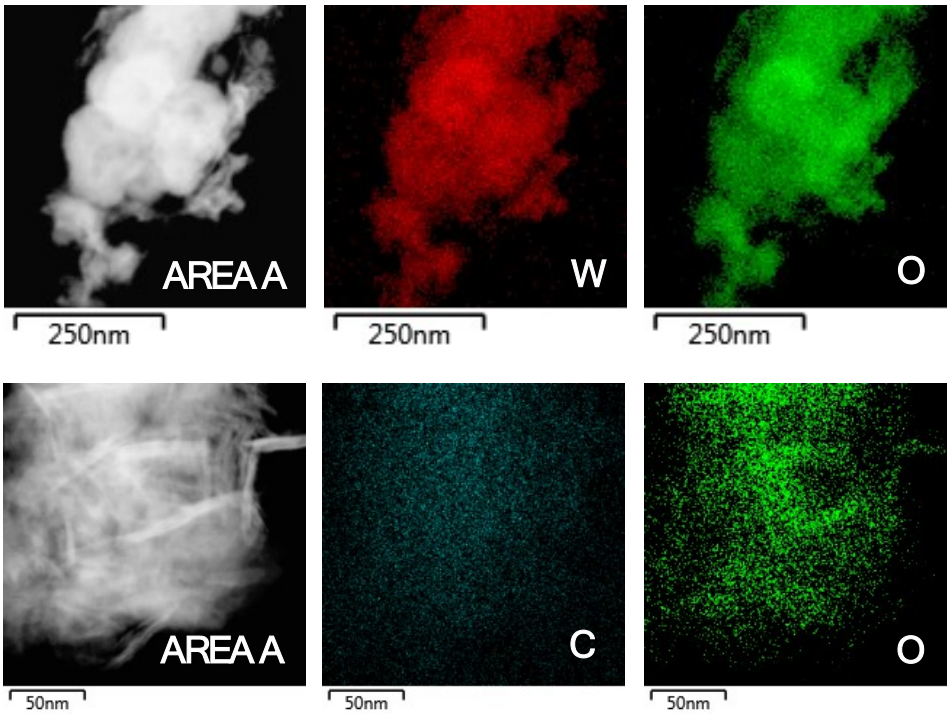

Figure SI - 5. STEM images of two regions of WO_3GO_180°C-0min sample and EDS mapping.

XRD patterns of replicates

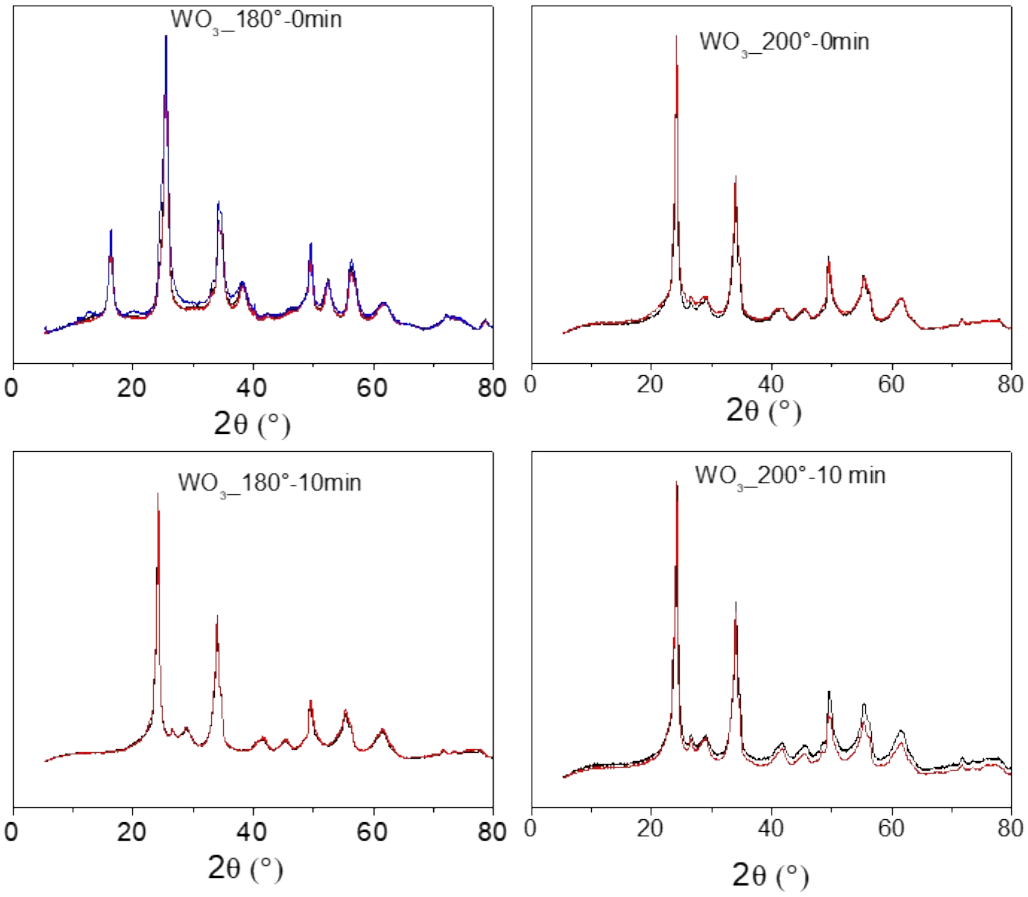

Figure SI - 6. XRD patterns of WO_3_180°C-0min, WO_3_180°C-10min, WO_3_200°C-0min and WO_3_200°C-10min replicates.

Thermal Gravimetry analysis

WO_3_180°C-0min (Figure SI - 5a) shows the highest weight loss of water among all materials (around 8%). The increased amount of adsorbed water is probably related to the chemically combined water of the hexagonal structure $WO_3.H_2O$ (Figure 2 - XRD) [16]. The second weight loss (3%) occurs around 450 °C and 550 °C, the temperature required to convert the hexagonal to monoclinic structure [17,18]. For this sample, the total weight loss up to 800°C was around 12.5%.

WO_3_180°C-10min (Figure SI - 5b) showed a weight loss significantly smaller (around 5%) up to 300 °C. The lower amount of adsorbed water, compared to the WO_3_180°C-0min, is consistent with the structural differences. Accordingly, the XRD pattern of the WO_3_180°C-10min exhibits a monoclinic structure. The second slight weight loss, around 450°C, can be ascribed to the partial conversion of residual $WO_3.H_2O$ (Figure 4 - XRD) into monoclinic WO_3. For this sample, the total weight loss is 12.5%.

Both WO_3_200°C-0min and WO_3_200°C-10min (Figure SI – 5 c and Figure SI – 5 d) have only shown significant weight loss up to 300 °C. For the WO_3_200°C-0min, the weight loss was around 8%, whereas, for the WO_3_200°C-10min, it was about 3.5%. However, WO_3_200°C-10min is probably more structurally stable since it exhibited a flat region after 350°C [19].

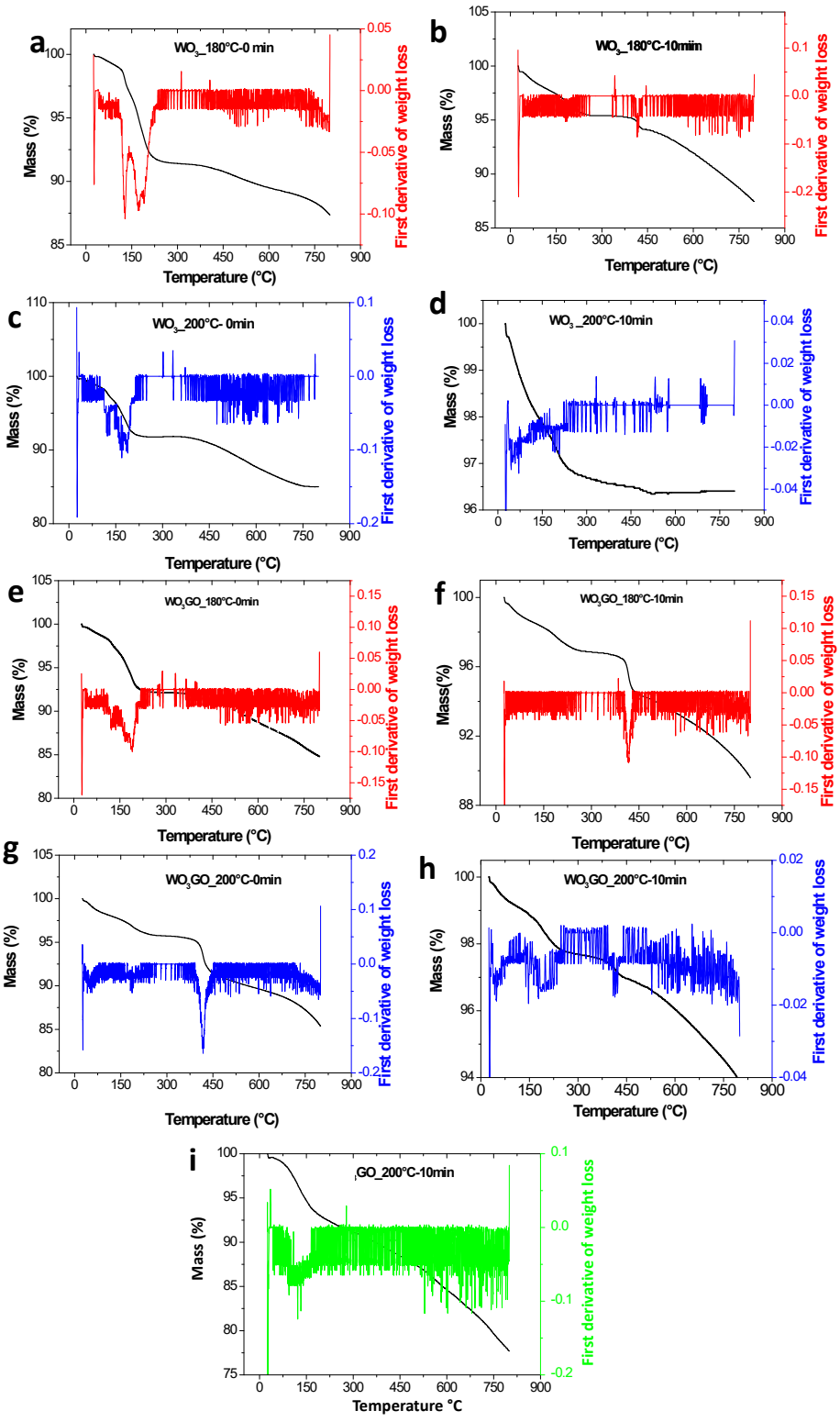

Figure SI - 7. Thermal gravimetry analysis (TGA) and first derivative of samples synthesized in (a) WO_3_180°C-0min, (b) WO_3_180°C-10min, (c) WO_3_200°C-0min, (d) WO_3_200°C-10min, (e) WO_3GO_180°C-0min, (f) WO_3GO_180°C-10min, (g) WO_3GO_200°C-0min and (h) WO_3GO_200°C-10min, (i) GO_200°C-10min

Samples modified with GO have shown a similar behavior (Figure SI – 7 e, f, g and h), within a first weight loss up to 300 °C and another event between 400 and 550° C. Again, the sample WO_3GO_180°C-0min (Figure SI - 7e), that previously exhibited a diffractogram of hexagonal structure $WO_3.H_2O$ (Figure 2 b), showed a significant weight loss up to 300 °C. The second event, around 500 °C, could be associated with converting to a monoclinic structure and a partial thermal decomposition of graphene oxide since the total weight loss was around 15%. On the other hand, WO_3GO_180°C-10min (Figure SI – 5 f) had only 3.5% of weight loss up to 300 °C. Between 400 °C and 550 °C, the loss was around 4%, probably related to graphene decomposition. The total weight loss was 9.5%. WO_3GO_200°C-0min (Figure SI - 7 g) exhibited 4.5% of weight loss up to 300 °C and around 5% between 400 °C and 550 °C, again the total weight loss was about 15%. WO_3GO_200°C-10min (Figure SI – 7 h) exhibited a weight loss of 3% up to 300 °C, around 2% between 400 °C and 550 °C with a total loss of 6%. For all samples containing GO, it is observed a continuous weight loss of up to 800 °C, which may be ascribed to the GO decomposition. It was also observed for GO_200°C-10min (Figure SI – 7 i), up to 300°C it had around 8% of weight loss that might be associated with adsorbed water and then, there was a continuous weight loss associated with graphene decomposition of 23% in total.

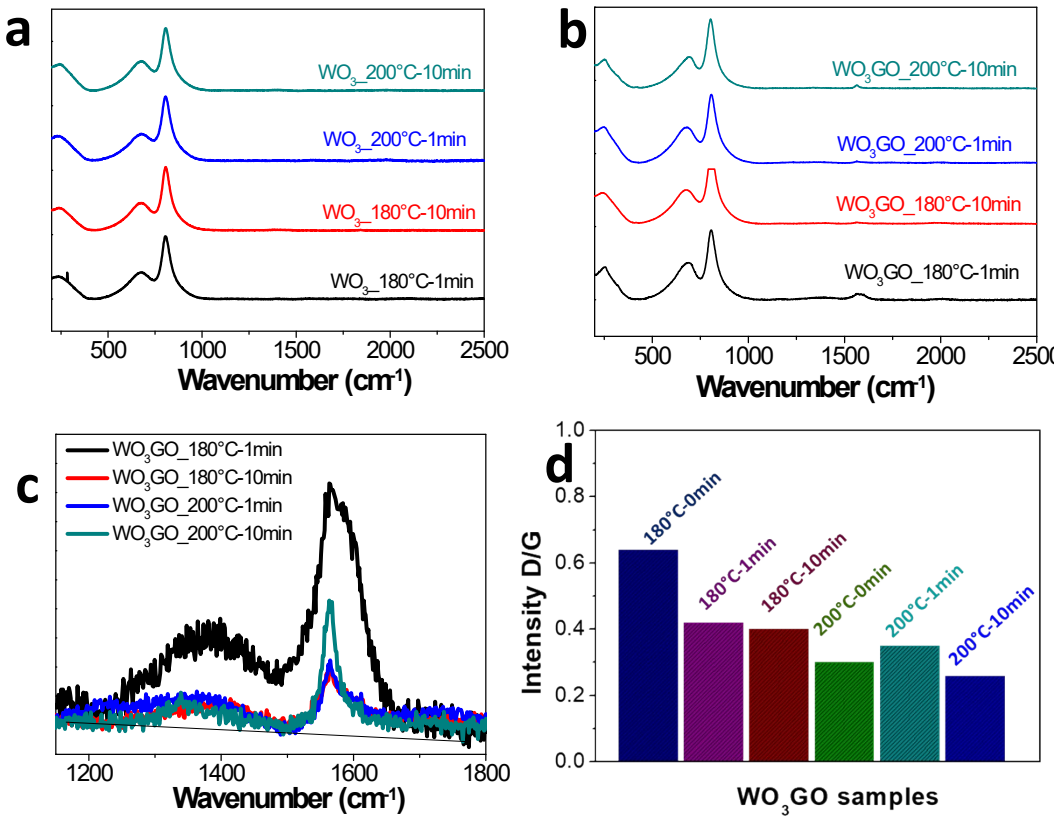

Figure SI - 8. Raman of (a) WO_3, (b) WO_3GO, (c) inset of WO_3GO and (d) comparison of D/G intensity between the samples.

FTIR of WO_3(GO) samples

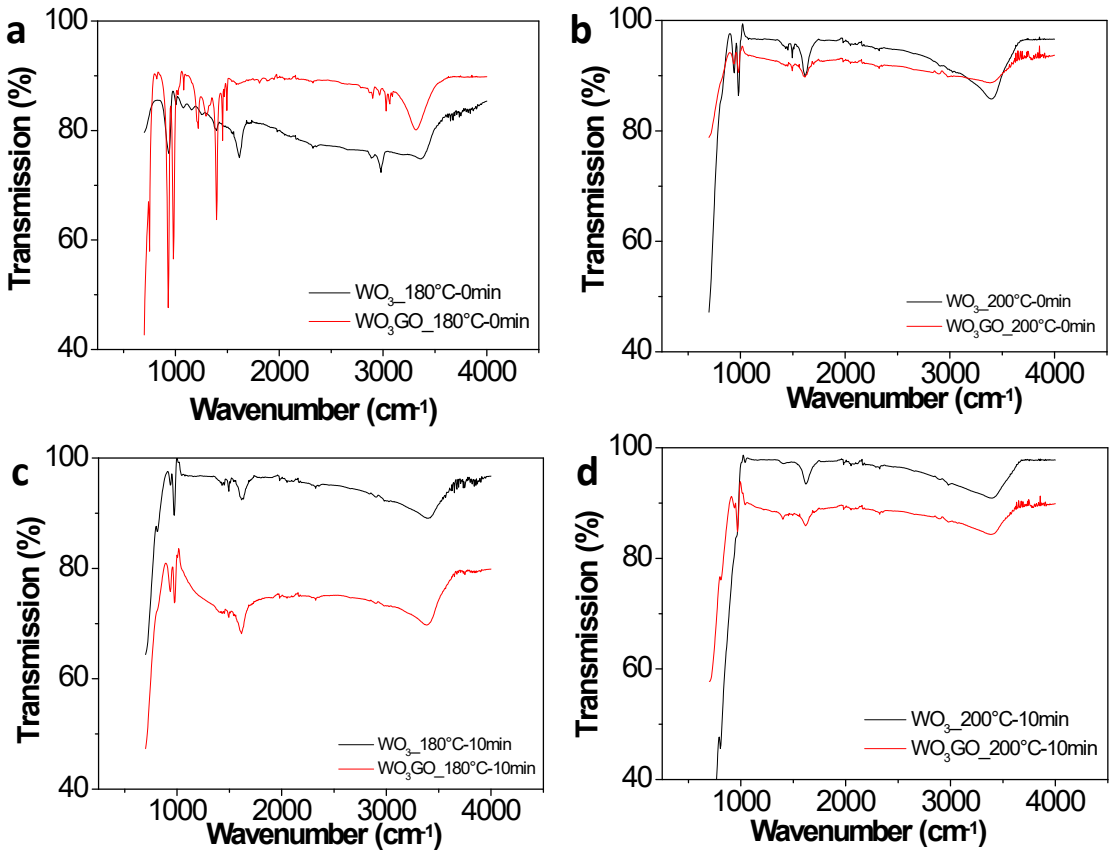

Figure SI - 9. FTIR of (a) WO_3_180°C-0min and WO_3GO_180°C-0min, (b) WO_3_200°C-0min and WO_3GO_200°C-0min, (c) WO_3_180°C-10min and WO_3GO_180°C-10min and (d) WO_3_200°C-10min and WO_3GO_200°C-10min

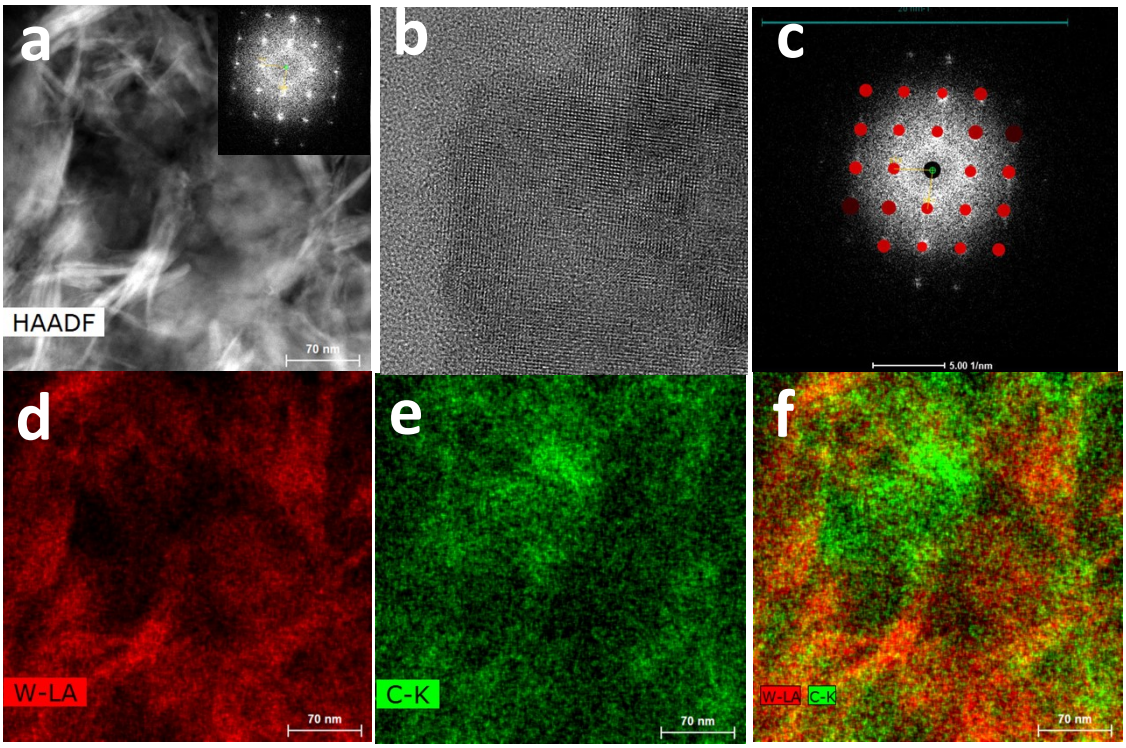

Figure SI - 10. (a) HAADF-STEM micrograph of WO_3GO_180°C-10min with inset FTT, (b) HRTEM image of the sample, (c) FFT fitting with the schematic diagram of monoclinic WO_3 pattern, HAADF-STEM image coupled with EDX of the sample monitoring (d) $W_{L\alpha}$, (e) $C_{K\alpha}$ and (f) $W_{L\alpha}$ and $C_{K\alpha}$.

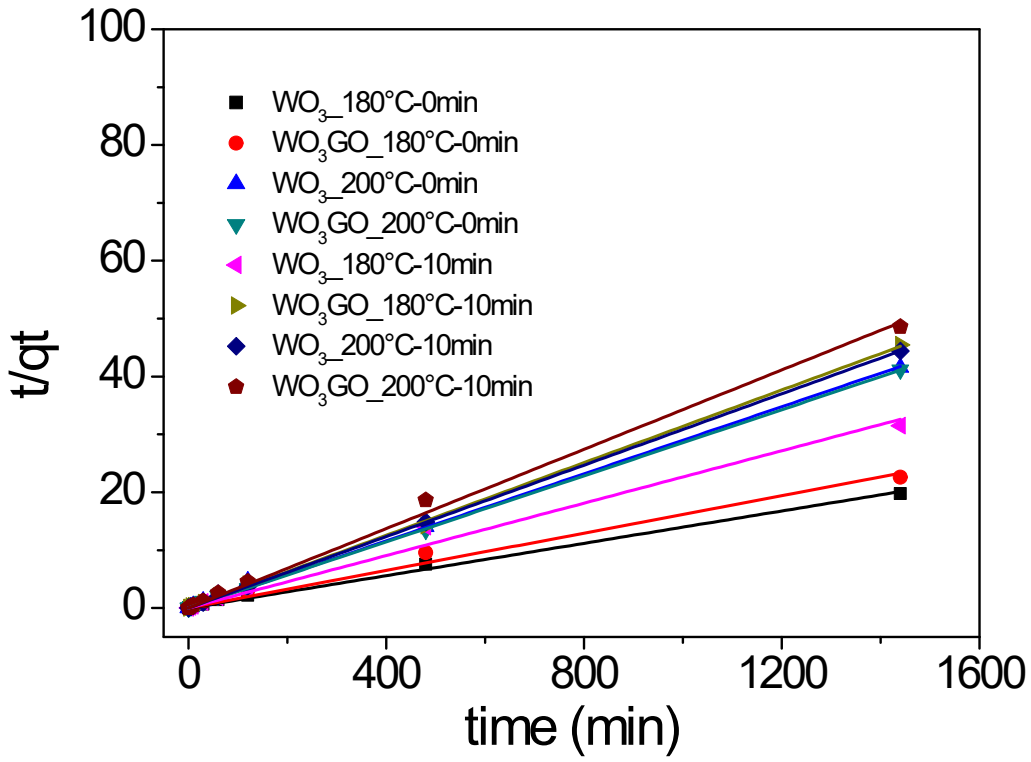

Figure SI - 11. Pseudo-second order kinetics for MB adsorption using WO_3_180°C-0min, WO_3GO_180°C-0min, WO_3_180°C-10min, WO_3GO_180°C-10min, WO_3_200°C-0min, WO_3GO_200°C-0min WO_3_200°C-10min and WO_3GO_200°C-10min as adsorbents.

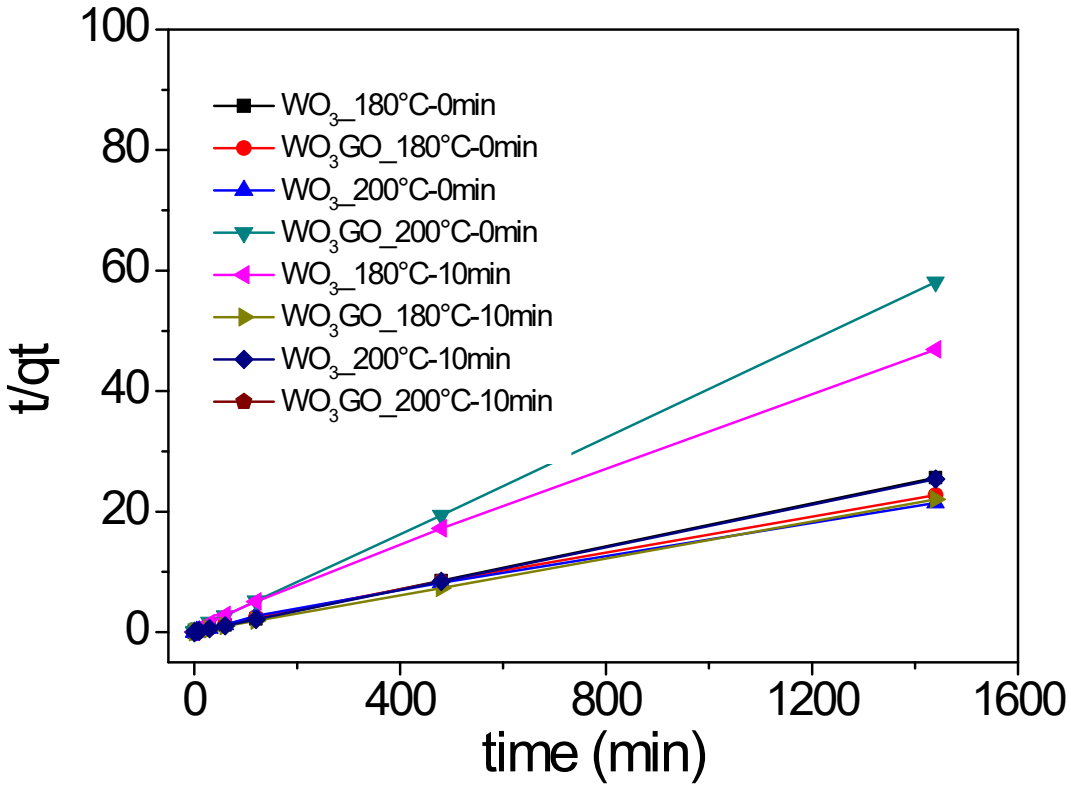

Figure SI - 12. Pseudo-second order kinetics for RhB adsorption using WO_3_180°C-0min, WO_3GO_180°C-0min, WO_3_180°C-10min, WO_3GO_180°C-10min, WO_3_200°C-0min, WO_3GO_200°C-0min WO_3_200°C-10min and WO_3GO_200°C-10min as adsorbents.

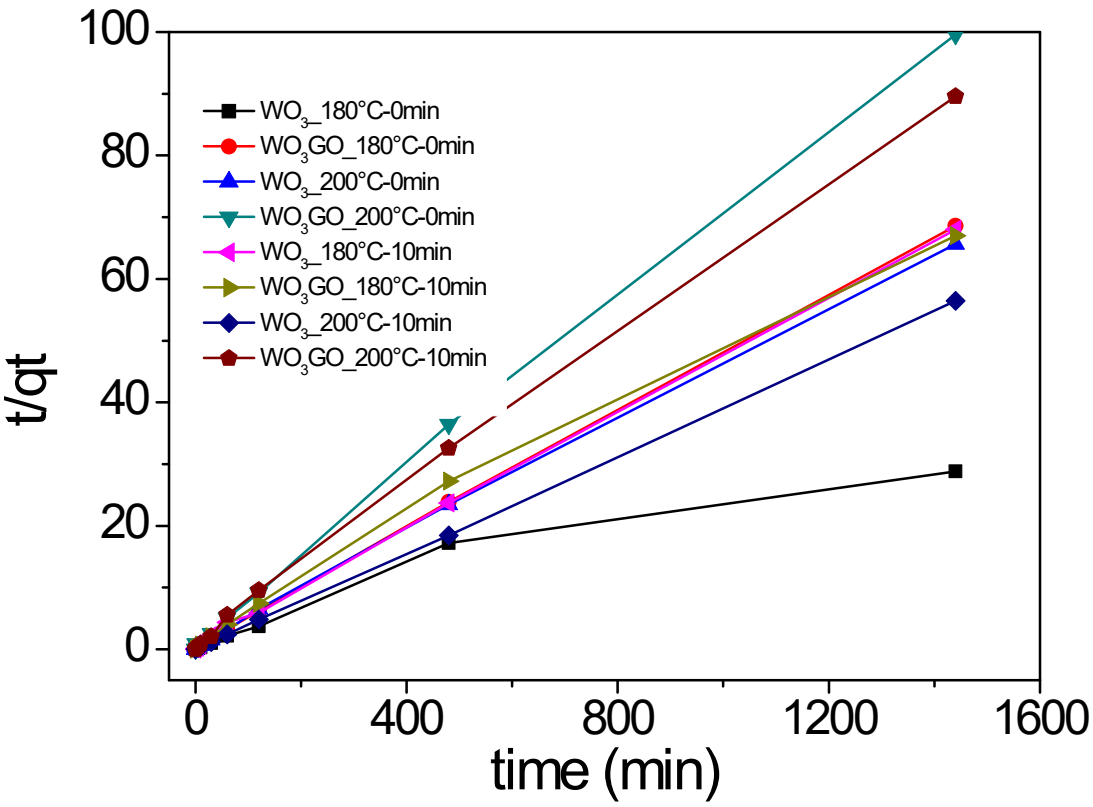

Figure SI - 13. Pseudo-second order kinetics for MO adsorption using WO_3_180°C-0min, WO_3GO_180°C-0min, WO_3_180°C-10min, WO_3GO_180°C-10min, WO_3_200°C-0min, WO_3GO_200°C-0min WO_3_200°C-10min and WO_3GO_200°C-10min as adsorbents.

(1) Olliges-Stadler, I.; Stötzel, J.; Koziej, D.; Rossell, M. D.; Grunwaldt, J.-D.; Nachtegaal, M.; Frahm, R.; Niederberger, M. Study of the Chemical Mechanism Involved in the Formation of Tungstite in Benzyl Alcohol by the Advanced QEXAFS Technique. *Chemistry – A European Journal* **2012**, *18* (8), 2305–2312. https://doi.org/https://doi.org/10.1002/chem.201101514.

(2) Hilaire, S.; Süess, M. J.; Kränzlin, N.; Bieńkowski, K.; Solarska, R.; Augustyński, J.; Niederberger, M. Microwave-Assisted Nonaqueous Synthesis of WO3 Nanoparticles for Crystallographically Oriented Photoanodes for Water Splitting. *J Mater Chem A Mater* **2014**, *2* (48), 20530–20537. https://doi.org/10.1039/C4TA04793A.

(3) Jeevitha, G.; Abhinayaa, R.; Mangalaraj, D.; Ponpandian, N.; Meena, P.; Mounasamy, V.; Madanagurusamy, S. Porous Reduced Graphene Oxide (RGO)/WO 3 Nanocomposites for the Enhanced Detection of NH 3 at Room Temperature. *Nanoscale Adv* **2019**, *1* (5), 1799–1811.

(4) Su, P.-G.; Peng, S.-L. Fabrication and NO2 Gas-Sensing Properties of Reduced Graphene Oxide/WO3 Nanocomposite Films. *Talanta* **2015**, *132*, 398–405. https://doi.org/https://doi.org/10.1016/j.talanta.2014.09.034.

(5) Huang, H.; Yue, Z.; Li, G.; Wang, X.; Huang, J.; Du, Y.; Yang, P. Ultraviolet-Assisted Preparation of Mesoporous WO3/Reduced Graphene Oxide Composites: Superior Interfacial Contacts and Enhanced Photocatalysis. *J Mater Chem A Mater* **2013**, *1* (47), 15110–15116. https://doi.org/10.1039/C3TA13433D.

(6) Markandan, K.; Chin, J. K.; Tan, M. T. T. Recent Progress in Graphene Based Ceramic Composites: A Review. *J Mater Res* **2017**, *32* (1), 84–106. https://doi.org/10.1557/jmr.2016.390.

(7) Jakhar, R.; Yap, J. E.; Joshi, R. Microwave Reduction of Graphene Oxide. *Carbon N Y* **2020**, *170*, 277–293. https://doi.org/https://doi.org/10.1016/j.carbon.2020.08.034.

(8) Chen, W.; Yan, L.; Bangal, P. R. Preparation of Graphene by the Rapid and Mild Thermal Reduction of Graphene Oxide Induced by Microwaves. *Carbon N Y* **2010**, *48* (4), 1146–1152. https://doi.org/https://doi.org/10.1016/j.carbon.2009.11.037.

(9) Lavin-Lopez, M. P.; Paton-Carrero, A.; Sanchez-Silva, L.; Valverde, J. L.; Romero, A. Influence of the Reduction Strategy in the Synthesis of Reduced Graphene Oxide. *Advanced Powder Technology* **2017**, *28* (12), 3195–3203. https://doi.org/https://doi.org/10.1016/j.apt.2017.09.032.

(10) Nagaraju, P.; Alsalme, A.; Alkathiri, A. M.; Jayavel, R. Rapid Synthesis of WO3/Graphene Nanocomposite via in-Situ Microwave Method with Improved Electrochemical Properties. *Journal of Physics and Chemistry of Solids* **2018**, *120*, 250–260. https://doi.org/https://doi.org/10.1016/j.jpcs.2018.04.046.

(11) Bao, Y.; Guo, H.; Jiang, L.; Liu, Z.; Qu, J.; Zhang, C.; Jia, X.; Chen, K. Heterostructured WO3/RGO/Protonated g-C3N4 Three-Layer Nanosheets for Enhanced Visible-Light Photocatalytic Activity. *Appl Surf Sci* **2019**, *496*, 143639. https://doi.org/https://doi.org/10.1016/j.apsusc.2019.143639.

(12) Amano, F.; Ishinaga, E.; Yamakata, A. Effect of Particle Size on the Photocatalytic Activity of WO3 Particles for Water Oxidation. *The Journal of Physical Chemistry C* **2013**, *117* (44), 22584–22590. https://doi.org/10.1021/jp408446u.

(13) Sing, K. S. W. J. Rouqerol and T. Siemieniewska. *Pure Appl. Chem.* **1985**, *57*, 603.

(14) Malefane, M. E.; Ntsendwana, B.; Mafa, P. J.; Mabuba, N.; Feleni, U.; Kuvarega, A. T. In-Situ Synthesis of Tetraphenylporphyrin/Tungsten (VI) Oxide/Reduced Graphene Oxide (TPP/WO3/RGO) Nanocomposite for Visible Light Photocatalytic Degradation of Acid Blue 25. *ChemistrySelect* **2019**, *4* (29), 8379–8389. https://doi.org/https://doi.org/10.1002/slct.201901589.

(15) Salama, T. M.; Morsy, M.; Abou Shahba, R. M.; Mohamed, S. H.; Mohamed, M. M. Synthesis of Graphene Oxide Interspersed in Hexagonal WO3 Nanorods for High-Efficiency Visible-Light Driven Photocatalysis and NH3 Gas Sensing. *Front Chem* **2019**, *7*, 722.

(16) Li, R.; Hu, F.; Bao, Q.; Bao, S.; Qiao, Y.; Yu, S.; Guo, J.; Li, C. M. Enhancement of Photoelectric Response of Bacteriorhodopsin by Multilayered WO3·H2O Nanocrystals/PVA Membrane. *Chemical Communications* **2010**, *46* (5), 689–691. https://doi.org/10.1039/B923354G.

(17) Szilágyi, I.; Pfeifer, J.; Balázsi, C.; Tóth, A.; Varga-Josepovits, K.; Madarász, J.; Pokol, G. Thermal Stability of Hexagonal Tungsten Trioxide in Air. *J Therm Anal Calorim* **2008**, *94* (2), 499–505.

(18) Zheng, J. Y.; Song, G.; Hong, J.; Van, T. K.; Pawar, A. U.; Kim, D. Y.; Kim, C. W.; Haider, Z.; Kang, Y. S. Facile Fabrication of WO3 Nanoplates Thin Films with Dominant Crystal Facet of (002) for Water Splitting. *Cryst Growth Des* **2014**, *14* (11), 6057–6066. https://doi.org/10.1021/cg5012154.

(19) Gotić, M.; Ivanda, M.; Popović, S.; Musić, S. Synthesis of Tungsten Trioxide Hydrates and Their Structural Properties. *Materials Science and Engineering: B* **2000**, *77* (2), 193–201. https://doi.org/https://doi.org/10.1016/S0921-5107(00)00488-8.